ARL-RR-7 AR-008-365

DEPARTMENT OF DEFENCE

DEFENCE SCIENCE AND TECHNOLOGY ORGANISATION

AERONAUTICAL RESEARCH LABORATORY

MELBOURNE, VICTORIA

Research Report 7

MATHEMATICAL MODELLING OF BONDED FIBRE-COMPOSITE REPAIRS TO AIRCRAFT

by

P.D. CHALKLEY

Approved for public release.

MAY 1993

AR-008-365

DEPARTMENT OF DEFENCE
DEFENCE SCIENCE AND TECHNOLOGY ORGANISATION
AERONAUTICAL RESEARCH LABORATORY

Research Report 7

MATHEMATICAL MODELLING OF BONDED FIBRE-COMPOSITE REPAIRS TO AIRCRAFT

by

P.D. CHALKLEY

SUMMARY

DTIC QUALITY INSPECTED 3

Bonded fibre-composite doublers are increasingly being used to reinforce and/or repair damaged or underdesigned metallic aircraft structure. This trend will continue as the average age of Australian civilian and military aircraft increases. Two mathematical models of the stress state in bonded doublers are presented in this report: the end-tapered double-lap joint and the stepped double-lap joint. The mathematical development of the two models is detailed and the fidelity of the predicted stress states compared with that obtained from finite element analyses and experiment.

DSTO AUSTRALIA

POSTAL ADDRESS: **Director, Aeronautical Research Laboratory,
506 Lorimer Street, Fishermens Bend, 3207
Victoria, Australia.**

TABLE OF CONTENTS

1. INTRODUCTION

Aging aircraft, both civilian and military, are prone to various types of deterioration and damage in their metallic components including general corrosion and cracking due to stress corrosion and fatigue. A technique pioneered at ARL[1] to extend the life of these aircraft is to bond fibre-composite reinforcements, such as boron/epoxy or graphite epoxy, over the damaged regions. In demanding situations, such as highly-stressed thick-section repairs, accurate methods of design and analysis are needed. This report details the development of two mathematical models for the adhesive shear-strain distribution in a scarfed repair: the end-tapered double-lap joint (Figure 1a) and the stepped double-lap joint (Figure 1b). These two joints are idealised representations of an end-tapered repair. An actual end-tapered repair or doubler, such as the ARL[2] developed F-111 wing-pivot-fitting (WPF) doubler (Figure 2), has a geometry as shown in Figure 1c, where after lay-up the doubler has been inverted and the outer plies bent over by pressure in an autoclave. Also in this report is a comparison between the mathematical model developed herein and a finite element (FE) analysis for both the end-tapered and the stepped double-lap joint. Finally a comparison is made between the measured strains in the outer adherend of a boron doubler (Figure 1c) and the strains predicted by the models of the end-tapered and the stepped double-lap joints.

The primary reason for tapering the ends of a composite doubler is to reduce the peel and shear stress, which arises there due to the load transfer conditions. A high peel stress (tensile stress that acts transverse to the plane of the bond) is detrimental because the interlaminar tensile strength of a fibre composite lay-up is typically less than 10% of its longitudinal tensile strength. For example, the longitudinal tensile strength[3] of unidirectional boron/epoxy is 1260 MPa whereas its interlaminar tensile strength is only 61 MPa - and the ratio of interlaminar to longitudinal toughness is even smaller than that of the strengths. Adhesives are also susceptible to failure induced by peel stresses. Tapering the ends reduces the adhesive shear-stress concentration at the ends of the doubler and hence also reduces the peel stress resulting from the unbalanced shear stress acting on the doubler. An optimum taper angle is generally about three degrees since this gives an adequate degree of stress relief while ensuring the size of the doubler is not too great. The modelling of the

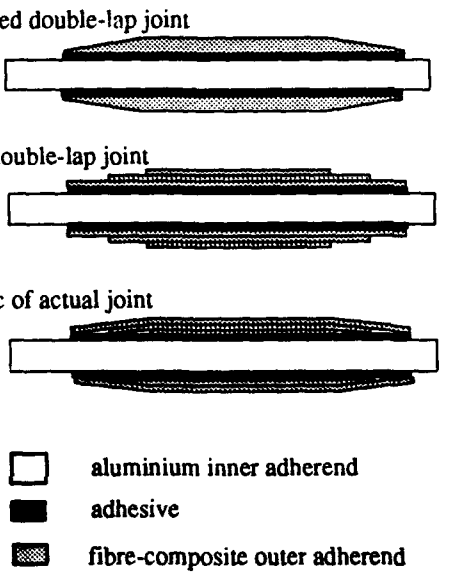

Figure 1

Schematic of the Two Mathematical Models and an Actual Doubler

peel-stress distribution is a more difficult mathematical problem and is not addressed in this report, however, minimising the shear will also minimise the peel stress.

The application of doublers to an aircraft structure can induce some bending due to the added eccentricity of the load path. However, most aircraft structures have supports that act to reduce this bending. For example, the WPF of the F-111 (Figure 2) has stiffeners and shear webs and is bolted to the sub-structure. The strength of the single-sided

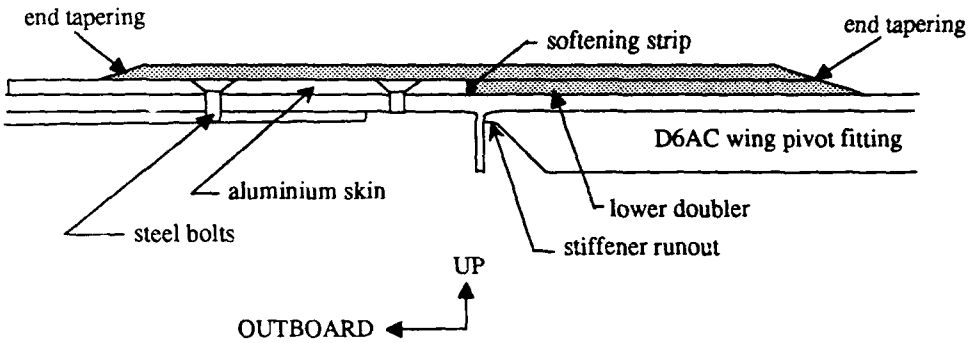

Figure 2. F-111 Doubler-Section Looking Aft on Right Wing.

end-tapered joint will then approach that of the end-tapered double-lap joint. Analysis of the single-sided end-tapered doubler can then be approximated by considering either the idealised geometry of the end-tapered double-lap joint (Figure 1a) or the stepped double-lap joint (Figure 1b) and by using a 'mechanics of solids' approach similar to that employed by Hart-Smith[4] in the analysis of the double-lap joint.

2. THE END-TAPERED DOUBLE-LAP JOINT

2.1. Elastic Analysis

2.1.1. Analytical Development

In this analysis, it is assumed that the adhesive deforms only by shear and that the adherends deform only by stretching in the longitudinal direction. This one-dimensional approach works reasonably well for the non-tapered double-lap joint[4] and should, given the reduced peel stresses, work even better for the end-tapered double-lap joint. Geometry and nomenclature for the end-tapered double-lap joint is shown in Figure 3. A fibre-composite outer adherend can be accommodated by using an effective modulus in the longitudinal direction. As most doublers employed at ARL have

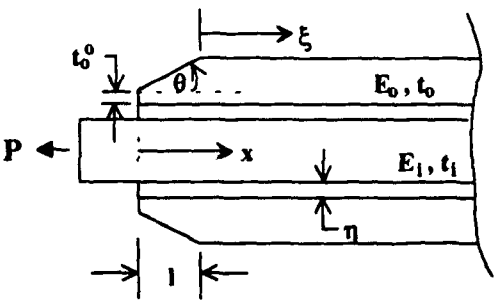

Figure 3. Geometry and Nomenclature for the End-tapered Double-Lap Joint

unidirectional reinforcement, the modulus along the fibre direction of a single ply can be used. To aid the analysis, the joint is divided into two regions: the tapered region from x=0 to x=l and the non-tapered region from x=l *to* x=∞ (or ξ =0 to ξ =∞). The differential equation describing adhesive deformation in the first region is derived below and the differential equation for the second region can be found from the first by putting the angle of taper to zero.

Force equilibrium in the horizontal direction dictates that:

$$\frac{dT_o}{dx} - \tau = 0, \tag{1}$$

and,

$$\frac{dT_i}{dx} + 2\tau = 0. \tag{2}$$

Here, τ is the adhesive shear stress and T_o and T_i are tractions in the outer and inner adherends respectively. The elastic stress-strain relations for the adherends are:

$$\frac{d\delta_o}{dx} = \frac{T_o}{E_o\left(x \tan\theta + t_o^o\right)} \tag{3}$$

and,

$$\frac{d\delta_i}{dx} = \frac{T_i}{E_i\, t_i}. \tag{4}$$

The terms δ_o and δ_i are the displacements of the outer and inner adherends respectively. The elastic shear-stress shear-strain relation for the adhesive is:

$$\tau = G\gamma \ . \tag{5}$$

In this analysis, the adhesive shear strain is averaged across the thickness of the adhesive layer:

$$\gamma = \frac{\delta_o - \delta_i}{\eta} \ . \tag{6}$$

Taking the derivative of equation 6 with respect to (w.r.t.) x and substituting in equations 3 and 4 yields:

$$\frac{d\gamma}{dx} = \frac{1}{\eta}\left[\frac{T_o}{E_o\left(x\tan\theta + t_o^o\right)} - \frac{T_i}{E_i t_i}\right]. \qquad (7)$$

Differentiating again w.r.t. x yields:

$$\frac{d^2\gamma}{dx^2} = \frac{1}{\eta}\left[\frac{E_o\left(x\tan\theta + t_o^o\right)\frac{dT_o}{dx} - E_o T_o \tan\theta}{E_o^2\left(x\tan\theta + t_o^o\right)^2} - \frac{dT_i}{dx}\frac{1}{E_i t_i}\right], \qquad (8)$$

but equations **1** and **2** imply $T_o = \int_0^\infty \tau\, dx$ and $\frac{dT_i}{dx} = -2\tau$, so that equation **8** becomes in terms of shear stress:

$$\frac{d^2\gamma}{dx^2} = \frac{1}{\eta}\left[\frac{E_o\left(x\tan\theta + t_o^o\right)\tau - E_o\tan\theta\int_0^\infty \tau(x)dx}{E_o^2\left(x\tan\theta + t_o^o\right)^2} + 2\tau\frac{1}{E_i t_i}\right]. \qquad (9)$$

Multiplying both sides of equation **9** by $E_o^2\left(x\tan\theta + t_o^o\right)^2$, substituting $\tau = G\gamma$, and taking the derivative w.r.t. x yields the third-order ordinary-differential equation:

$$\frac{d^3\gamma}{dx^3} + \frac{2\tan\theta}{x\tan\theta + t_o^o}\frac{d^2\gamma}{dx^2} = \frac{G}{\eta}\left[\frac{2}{E_i t_i} + \frac{1}{E_o\left(x\tan\theta + t_o^o\right)}\right]\frac{d\gamma}{dx}$$

$$+ \frac{G}{\eta}\frac{4\tan\theta}{E_i t_i\left(x\tan\theta + t_o^o\right)}\gamma. \qquad (10)$$

Equation **10** is probably not soluble in closed form. It is amenable, however, to a numerical solution using the NAG[1] subroutine D02HAF. This is a subroutine for solving boundary-value problems involving ordinary differential equations of arbitrary order. The equations are re-written as a system of simultaneous first-order differential equations and the problem solved by a shooting and matching technique.

---

[1] Numerical Algorithms Group library of mathematical subroutines.

The boundary condition at x=**0** is obtained from equation **7**:

$$\frac{d\gamma}{dx}(0) = -\frac{P}{\eta E_i t_i}. \tag{11}$$

The other two boundary conditions are derived by matching γ and γ' at x=**l** from the preceding solution with γ and γ' at ξ=0 from the solution for the non-tapered double-lap joint. The form of the solution for the non-tapered double-lap joint is:

$$\gamma_n(\xi) = \frac{P_l}{\eta E_i t_i \beta} e^{-\beta\xi}, \tag{12}$$

where the subscript **n** refers to the non-tapered double-lap joint and P_l is the load remaining at x=**l** to be transferred from the inner to the outer adherends at x=**l**.

The solution shown above for the non-tapered double-lap joint can be obtained from the previous equations by substituting $\theta = 0$ and $t_o^\circ = t_o$ in equation **8.** Then:

$$\frac{d^2\gamma_n}{dx^2} = \frac{1}{\eta}\left[\frac{1}{E_o t_o^\circ}\frac{dT_o}{dx} - \frac{1}{E_i t_i}\frac{dT_i}{dx}\right]. \tag{13}$$

Substituting the equilibrium equations **1** and **2** and equation **5** gives:

$$\frac{d^2\gamma_n}{dx^2} = \frac{G}{\eta}\left[\frac{1}{E_o t_o^\circ} + \frac{2}{E_i t_i}\right]\gamma_n,$$

$$= \beta^2\gamma_n, \tag{14}$$

where

$$\beta^2 = \frac{G}{\eta}\left[\frac{1}{E_o t_o^\circ} + \frac{2}{E_i t_i}\right]. \tag{15}$$

The solution of equation **14** over a semi-infinite domain is equation **12** above. The boundary condition $\gamma(\infty) = 0$ is implicit in this formulation. Solution over a finite domain, **p** say, is:

$$\gamma_n(\xi) = A\cosh(\beta(p-\xi)) + B\sinh(\beta(p-\xi)). \tag{16}$$

P_l in equation **12** is the load remaining at x=**l** to be transferred from the inner to the outer adherends and is given by:

$$P_l = T_i - P\frac{E_i t_i}{2E_o t_o + E_i t_i}. \tag{17}$$

The last term in equation 17 expresses the condition that at $x = \infty$ the load is distributed to each adherend according to its stiffness.

Matching at $x=l$ ($\xi=0$) implies that:

$$\gamma(l) = \gamma_n(0)\ ,$$

$$= \frac{P_l}{\eta E_i t_i \beta}, \tag{18}$$

and,

$$\frac{d\gamma}{dx}(l) = \frac{d\gamma_n}{d\xi}(0),$$

$$= -\frac{P_l}{\eta E_i t_i}\ . \tag{19}$$

Since P_l is not known ***a priori*** neither are the boundary conditions at $x=l$. Consequently, an iterative scheme was implemented on computer to solve the governing differential equation (equation **10**) and its boundary conditions (equations **11**, **18**, and **19**). The iterative scheme involved making repeated guesses at the parameter P_l until the load transferred to the outer adherends (which was found by integrating equation **1**) was equal to $P\frac{E_o t_o}{2E_o t_o + E_i t_i}$.

2.1.2. Comparison of the Elastic Model with an FE Analysis

An FE analysis of an end-tapered double-lap joint was set up in PAFEC. Only one quarter of the joint needed to be modelled due to the twofold symmetry of the joint. The adhesive and the adherends were modelled using eight-noded isoparametric elements. Previous experience in modelling double-lap joints dictated the need for four elements through the thickness of the adhesive layer to achieve convergence. Adhesive shear strains were calculated by subtracting the longitudinal displacements of nodes on either side of the adhesive layer and dividing through by the adhesive thickness. The adhesive shear strain is therefore averaged across the thickness, as in the analytical development, thus allowing proper comparison. The graphs that follow show the effect of varying joint parameters on the adhesive shear-strain distribution in the joint. Table 1 contains those joint parameters.

Parameter value	Figure 4	Figure 5	Figure 6	Figure 7
η (mm)	0.14-0.42	0.28	0.28	0.28
G (MPa)	600	600	600	600
E_o (MPa)	208,000	208,000	208,000	72,000-208,000
θ (degrees)	2.7	2.7	2.7-8.0	2.7
t_o^o (mm)	0.14	0.14-0.42	0.14	0.14
E_1 (MPa)	208,000	208,000	208,000	208,000
t_1 (mm)	6.36	6.36	6.36	6.36
l (mm)	27	27	27	27
P (N/mm)	2,300	2,300	2,300	2,300

Table 1.

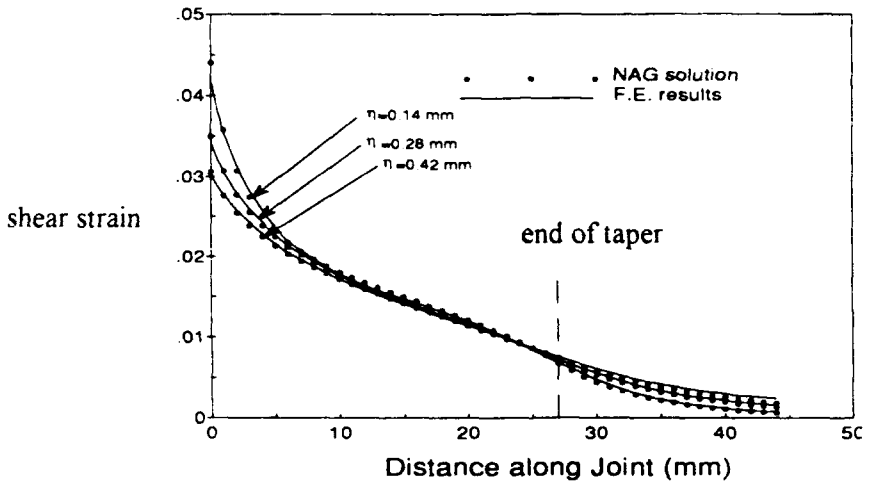

Figure 4.

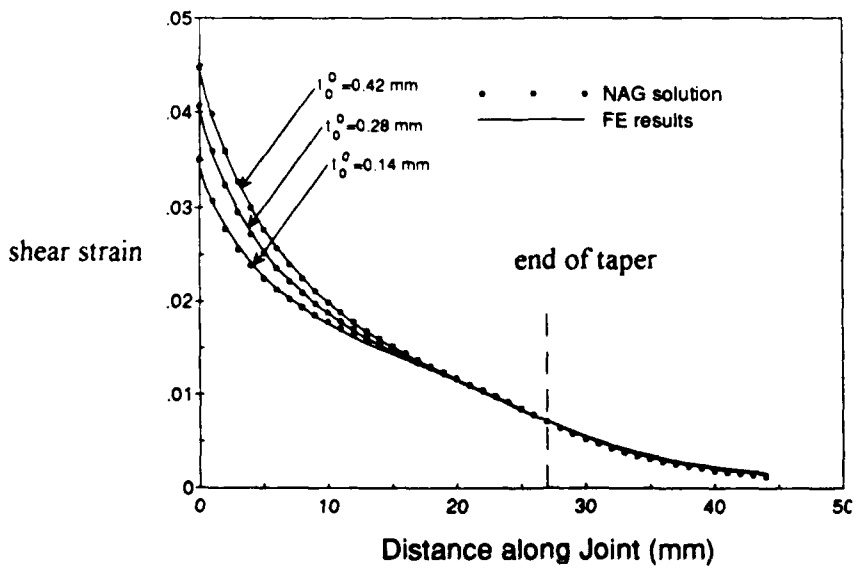

Figure 5.

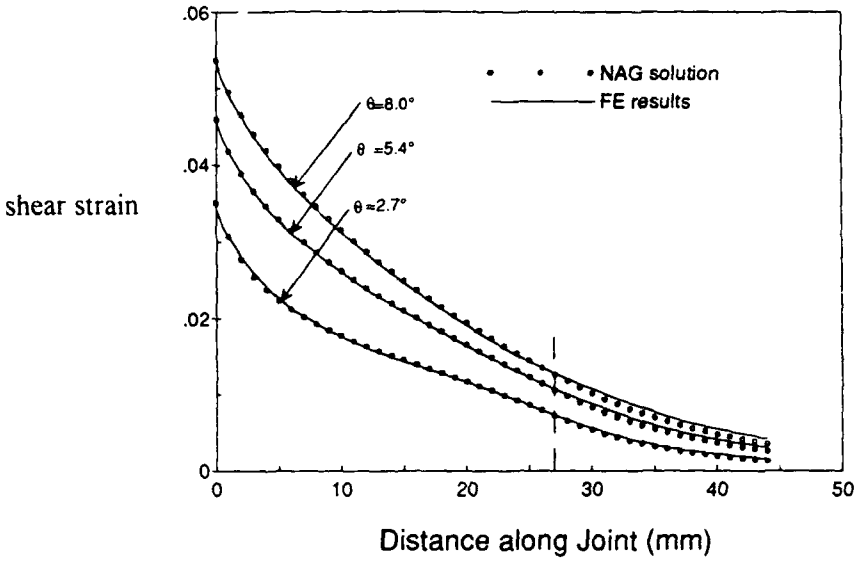

Figure 6.

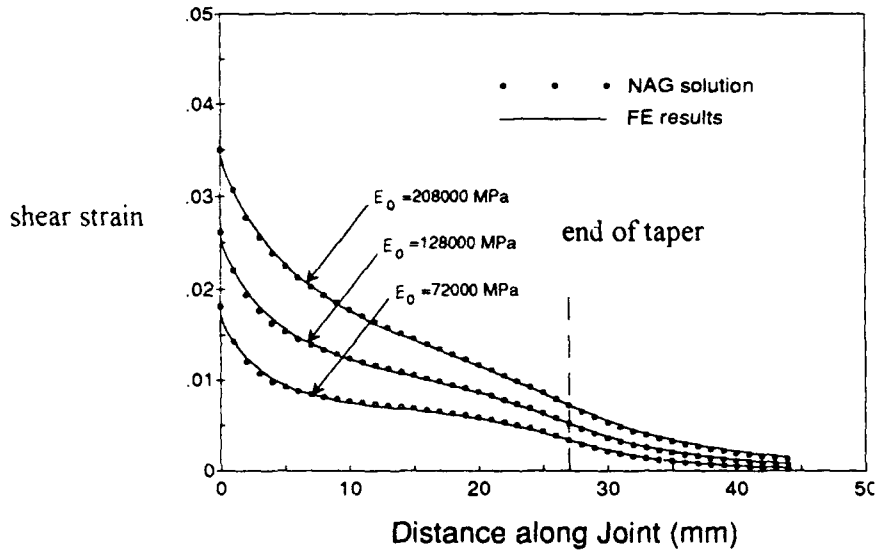

Figure 7.

Figures 4,5,6, and 7 show that the model of the end-tapered double-lap joint, assuming elastic adhesive deformation, is in excellent agreement with the finite-element analysis for a wide range of joint parameters.

2.1.3. An Approximate Analytical Solution: a First-Order Perturbation Solution

An approximate analytical solution to the differential equation governing elastic deformation of the adhesive (equation **10**) can be found by proposing a regular perturbation expansion of the shear strain:

$$\gamma(x) = \gamma_0(x) + \varepsilon\gamma_1(x) + \varepsilon^2\gamma_2(x) + \ldots\ldots \tag{20}$$

where the parameter ε is a small number much less than one. This parameter is associated with term ***tan*θ** in equation **10**. If the taper angle, **θ** , is very small then ***tan*θ** will also be small. Rewriting equation **10** in terms of ε gives:

$$\left(x\varepsilon + t_o^o\right)\gamma''' + 2\varepsilon\gamma'' = \frac{G}{\eta}\left[\frac{2}{E_i t_i}\left(x\varepsilon + t_o^o\right) + \frac{1}{E_o}\right]\gamma' + \frac{4G\varepsilon}{E_i t_i \eta}\gamma. \tag{21}$$

The first order perturbation expansion of the shear strain (i.e. the first two terms on the right hand side of equation **20**) is then substituted into equation **21** and terms with like powers of ε collected. The zero*th* order terms are:

$$t_o^o\gamma_0''' = \frac{G}{\eta}\left[\frac{2}{E_i t_i}\left(x\varepsilon + t_o^o\right) + \frac{1}{E_o}\right]\gamma_0'. \tag{22}$$

The relevant boundary conditions are:

$$\frac{d\gamma_0}{dx}(0) = \frac{-P}{\eta E_i t_i};$$

$$\gamma_0\left(l\right) = \frac{P_l}{\eta E_i t_i \beta_l};$$

$$\gamma_0'\left(l\right) = \frac{-P_l}{\eta E_i t_i}.$$

The parameter β_l is given by:

$$\beta_l = \left[\frac{G}{\eta}\left(\frac{2}{E_i t_i} + \frac{1}{E_o t_o}\right)\right]^{\frac{1}{2}}.$$

The zero*th* order function, γ_0, is then:

$$\gamma_0(x) = A\cosh\left[\beta_o\left(1-x\right)\right] + B\sinh\left[\beta_o\left(1-x\right)\right] + C. \tag{23}$$

The parameter β_o is given by:

$$\beta_o = \left[\frac{G}{\eta}\left(\frac{2}{E_i t_i} + \frac{1}{E_o t_o^o}\right)\right]^{\frac{1}{2}}.$$

The constants **A**, **B**, **C** are found by substituting the boundary conditions into equation **23**:

$$A=\frac{\cosh\left(\beta_o l\right)}{\beta_o \sinh\left(\beta_o l\right)}\frac{(P-P_l)}{\eta E_i t_i};$$

$$B=\frac{P_l}{\eta E_i t_i \beta_o};$$

$$C=B\frac{\beta_o}{\beta_l}-A.$$

Note that the parameter $\mathbf{P_l}$ is not yet determined. It is found by setting the integral of the shear stress equal to the load per-unit-width that has to be transferred from the inner to each outer adherend.

The first order terms found on substituting the perturbation expansion into equation **10** are:

$$\gamma_1'''t_o^\circ+x\gamma_0'''+2\gamma_0''=\frac{G}{\eta}\frac{2x}{E_i t_i}\gamma_0'+\frac{G}{\eta}\left(\frac{2t_o^\circ}{E_i t_i}+\frac{1}{E_o}\right)\gamma_1'+4\frac{G}{\eta}\frac{1}{E_i t_i}\gamma_0 \qquad (24)$$

The relevant boundary conditions are:

$$\gamma_1\left(1\right)=0;$$

$$\gamma_1'(0)=0;$$

$$\gamma_1'\left(1\right)=0.$$

The homogeneous solution to the above differential equation is:

$$\gamma_1^{hom}(x)=D\cosh\left[\beta_o\left(1-x\right)\right]+E\sinh\left[\beta_o\left(1-x\right)\right]+F. \qquad (25)$$

The particular solution to the above differential equation, having first substituted for $\gamma_0(x)$, is:

$$\gamma_1^{par}(x)=aa\,x+bb\,x\cosh\left[\beta_o\left(1-x\right)\right]+cc\,x\sinh\left[\beta_o\left(1-x\right)\right]+dd\,x^2\cosh\left[\beta_o\left(1-x\right)\right]$$

$$+ee\,x^2\sinh\left[\beta_o\left(1-x\right)\right]. \qquad (26)$$

The constants **aa, bb, e.t.c. are given by**:

$$aa=\frac{4G}{\eta E_i t_i}\frac{1}{\beta_o^2 t_o^o}C;$$

$$bb=\frac{1}{2\beta_o^2 t_o^o}\left[\left(-2\beta_o^2+\frac{4G}{\eta E_i t_i}\right)A+\left(\frac{-2\beta_o G\, t_o^o}{\eta E_i t_i}\right)B+6\beta_o\, t_o^o\, ee\right];$$

$$cc=\frac{1}{2\beta_o^2 t_o^o}\left[\left(-2\beta_o^2+\frac{4G}{\eta E_i t_i}\right)B+\left(\frac{-2\beta_o G\, t_o^o}{\eta E_i t_i}\right)A+6\beta_o\, t_o^o\, dd\right];$$

$$dd=\frac{\beta_o}{4t_o^o}B;$$

$$ee=\frac{\beta_o}{4t_o^o}A.$$

Since the constants **A**, **B**, **C** depend only on $\mathbf{P_1}$ the constants **aa**, **bb**, **cc**, e.t.c. depend only on $\mathbf{P_1}$. The constants **D**, **E**, and **F** can now be found by evaluating the boundary conditions for $\gamma_1(\mathbf{x})$. These boundary conditions give rise to three simultaneous equations in which **D**, **E**, and **F** can be solved for in terms of $\mathbf{P_1}$. Thus the solution is fully determined once $\mathbf{P_1}$ is found. $\mathbf{P_1}$ is found by setting:

$$\int_0^\infty \tau(x)dx=\frac{P\,E_o t_o}{2E_o t_o+E_i t_i}. \tag{27}$$

The term $\tau(\mathbf{x})$ is given, on $\mathbf{0<x<l}$, by:

$$\tau(x)=G\left(\gamma_0(x)+\varepsilon\gamma_1(x)\right), \tag{28}$$

and on $l< x < \infty$ by:

$$\tau(x)=\frac{P_1 G}{\eta E_i t_i \beta_1}\exp\left(-\beta_1 x\right). \tag{29}$$

Figure 8 shows a comparison of the numerical solution for the joint configuration that follows and the first-order perturbation solution.

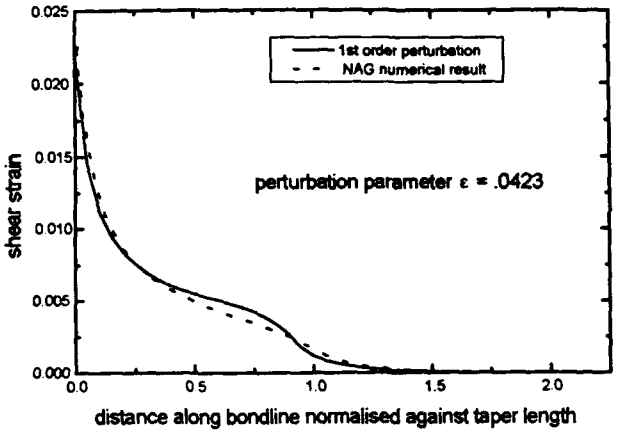

Figure 8.

η (mm)	G (MPa)	E_o (MPa)	t_o° (mm)	E_i (MPa)	t_i (mm)	θ (degrees)	l (mm)	P (N/mm)
0.14	700	208e3	0.13	71e3	6.36	2.42	27	500

Table 2.

The 1st order perturbation solution shows reasonable agreement with the more accurate numerical solution. A higher order perturbation expansion for the adhesive shear strain would be necessary to achieve a more accurate approximation.

2.2. Elastic/Perfectly-Plastic Analysis

2.2.1. Analytical Development

To obtain the solution for the adhesive shear-strain distribution in a joint deforming in an elastic/perfectly-plastic manner the tapered region must be divided into an elastic region and a plastic region. Firstly the adhesive shear-stress shear-strain curve is idealised as being elastic/perfectly-plastic.

In the plastic region a solution is obtained by setting $\tau(x)=\tau_p$ (the yield stress) in equation 9:

$$\frac{d^2\gamma}{dx^2} = \frac{1}{\eta}\left[\frac{\tau_p E_o t_o^o}{E_o^2\left(x\tan\theta + t_o^o\right)^2} + \frac{2\tau_p}{E_i t_i}\right]. \qquad (30)$$

Integrating equation **30** w.r.t. x yields:

$$\frac{d\gamma}{dx} = \frac{1}{\eta}\left[\frac{2\tau_p x}{E_i t_i} - \frac{\tau_p t_o^o}{E_o \tan\theta\left(x\tan\theta + t_o^o\right)}\right] + C. \qquad (31)$$

Integrating once again:

$$\gamma(x) = \frac{1}{\eta}\left[\frac{\tau_p x^2}{E_i t_i} - \frac{\tau_p t_o^o \ln\left(x\tan\theta + t_o^o\right)}{E_o \tan^2\theta}\right] + Cx + D. \qquad (32)$$

Applying the boundary condition given by equation **11** to equation **32** yields:

$$\gamma(x) = \frac{1}{\eta}\left[\frac{\tau_p x^2}{E_i t_i} - \frac{\tau_p t_o^o \ln\left(x\tan\theta + t_o^o\right)}{E_o \tan^2\theta}\right]$$

$$+\left[\frac{\tau_p}{\eta E_o \tan\theta} - \frac{P}{\eta E_i t_i}\right]x + D. \qquad (33)$$

As in the elastic analysis the other boundary conditions are found by matching. In this case, however, the adhesive in the tapered region can deform fully plastically or partly plastically and partly elastically. If the deformation in the taper is fully plastic then equation **33** is matched with the solution describing adhesive plasticity in the non-tapered double-lap joint at $x=l$. That solution is obtained by setting $\tan\theta = 0$ in equation **30** and integrating:

$$\frac{d^2\gamma_n}{d\xi^2} = \frac{\tau_p}{\eta}\left[\frac{1}{E_o t_o} + \frac{2}{E_i t_i}\right] = \frac{\tau_p \beta^2}{G}, \qquad (34)$$

and hence,

$$\gamma_n\left(\xi\right) = \frac{\tau_p \beta^2 \xi^2}{2G} + E\xi + F. \qquad (35)$$

This solution is then matched with that assuming adhesive elasticity in the non-tapered double-lap joint (equation **12**) at the plastic-to-elastic transition point. The location of this transition point is not known *a priori* and so an iterative scheme was again implemented on computer to find the full solution by making guesses at the starting strain.

If the adhesive deforms plastically for only part of the scarfed region then a different procedure is necessary. Equation **33** is now matched with the equation **10** (the solution assuming adhesive elasticity in the scarfed region) at the plastic-to-elastic transition point. At $x=l$ equation **10** is matched with the solution assuming adhesive elasticity in the non-tapered joint (equation **12**). A computerised iterative solution was again necessary to find the full solution.

2.3. An Upper and a Lower Bound for the Peak Shear Strain

It is desirable, from an engineering design viewpoint, to find a simple expression for both the upper and lower bound for the peak shear-strain in an end-tapered double-lap joint. A simple approach is to consider two separate double-lap joints. The joint used to estimate the upper bound would have an outer adherend thickness equal to $\mathbf{t_o}$ and the joint used to estimate the lower bound would have an outer thickness of $\mathbf{t_o}^\circ$. By comparing the results from the end-tapered double-lap joint model (with fixed values of $\mathbf{t_o}$ and $\mathbf{t_o}^\circ$ but varying values of θ) with the results from the two double-lap joints the usefulness of the estimates for the upper and lower bounds can be evaluated. To be useful, at small values of θ the peak shear-strain should approach the lower bound and at large values of θ it should approach the upper bound. Two cases were investigated: elastic and elastic/perfectly-plastic adhesive deformation.

2.3.1. Assuming Elastic Adhesive Deformation.

Figure 9 shows the variation of peak shear strain with taper angle when the adhesive is assumed to deform elastically. The joint parameters are as for Figure 4 with these exceptions: **P**=2000 N/mm and η=0.14mm.

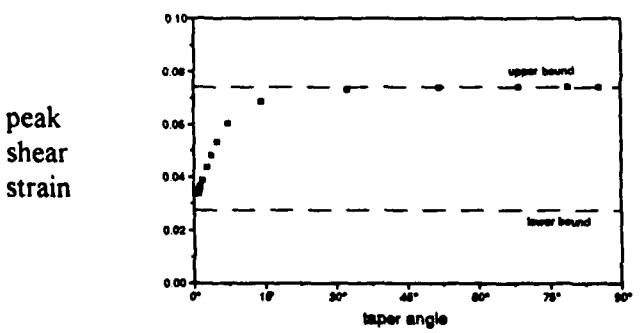

Figure 9.

The upper bound provides a sound upper limit for the peak shear strain at large angles of taper but the lower bound underestimates the peak shear strain at small angles of taper. Taper angles in a repair are typically 2-4° and hence the upper bound may be too conservative to be used for design purposes. Likewise, the lower bound may be too low to be used for design purposes (e.g. for a taper angle of 2.7° the actual peak shear strain is 58% greater than the lower bound).

2.3.2. Assuming Elastic/Perfectly-Plastic Adhesive Behaviour

When the adhesive is allowed to deform in an elastic/plastic manner a similar graph is obtained (Figure 10). In this case the lower bound greatly underestimates the peak shear strain. Loads high enough to cause adhesive plasticity, however, are rarely encountered. Table 3 contains the parameters for the joint.

P (N/mm)	Ei (MPa)	ti (mm)	Eo (MPa)	t_o° (mm)	t_o (mm)	G (MPa)	τ_p (MPa)	η (mm)
4,000	71,000	6.36	205,000	0.13	1.27	750	37	0.13

Table 3.

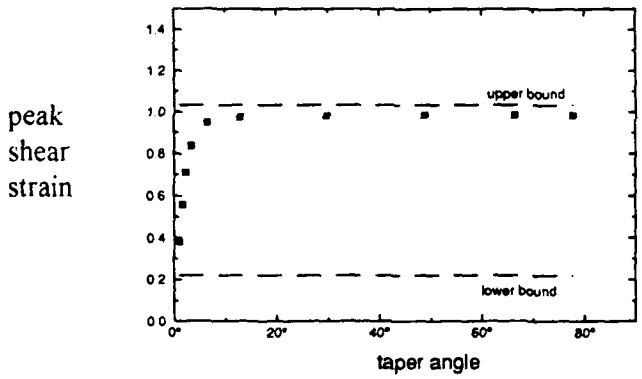

Figure 10.

3. THE STEPPED DOUBLE-LAP JOINT

3.1. Elastic Analysis

3.1.1. Analytical Development

This model of the stepped double-lap joint (Figure 1b) applies the solution for the double-lap joint (equation 16) to each step. Each ply of the outer adherend is assumed to be of step length **l**, thickness t_o, and Young's modulus E_o. A joint of this type could be made by stepping the plies of a fibre composite lay-up to form the outer adherends. The form of the solution on the ***k***th step is:

$$\gamma_k\left(\xi\right)=A_k\sinh\left(\beta_k\xi\right)+B_k\cosh\left(\beta_k\xi\right), \tag{36}$$

where ξ is the local coordinate for each step and where

$$\beta_k^2=\frac{G}{\eta}\left(\frac{1}{E_o t_o k}+\frac{2}{E_i t_i}\right). \tag{37}$$

The boundary condition given by equation **11** applies to the first step:

$$\frac{d\gamma_1}{d\xi}(0)=-\frac{P}{\eta E_i t_i}$$

$$=A_1\beta_1. \tag{38}$$

At the end of each step, of length **l**, continuity of the shear strain must be enforced, though the derivative of the shear strain may not necessarily be continuous since the profile of the outer adherend is not smooth.

Therefore,

$$\gamma_k(l)=\gamma_{k+1}(0) \tag{39}$$

or,

$$B_{k+1}=A_k\sinh\left(\beta_k l\right)+B_k\cosh\left(\beta_k l\right). \tag{40}$$

At the start of each step, the derivative of the shear strain is:

$$\frac{d\gamma_k}{d\xi}(0)=\frac{1}{\eta}\left(\frac{T_o}{E_o t_o k}-\frac{T_i}{E_i t_i}\right). \tag{41}$$

This equation can be derived from equation 7 by setting $\tan\theta=0$ and $t_o^o=kt_o$.

If the load transferred from the inner to each outer adherend over the ***k***th step is F_k then at the start of the ***k+1***th step the tractions are:

$$T_o=\sum_{j=1}^{k}F_j, \tag{42}$$

and,

$$T_i = P - 2\sum_{j=1}^{k} F_j \,. \tag{43}$$

Therefore, from equation **41**:

$$A_k\beta_k = \frac{d\gamma_k}{d\xi}(0) = \frac{1}{\eta}\left(\frac{\Sigma F_j}{E_o t_o k} - \frac{P - 2\Sigma F_j}{E_i t_i}\right), \tag{44}$$

where $\mathbf{F_k}$ is given by integrating equation **36**:

$$F_k = G\left\{A_k\left[\cosh\left(\beta_k l\right) - 1\right] + B_k \sinh\left(\beta_k l\right)\right\}. \tag{45}$$

Thus if $\mathbf{B_1}$ in equation **36** is known then all the coefficients $\mathbf{A_k}$ and $\mathbf{B_k}$ can be found. At the start of the last step the shear strain must also be continuous. The form of the solution for this last (*n*th) step is as for equation **12**:

$$\gamma\left(\xi\right) = \frac{P_1}{\eta E_i t_i \beta_n} e^{-\beta_n \xi}. \tag{46}$$

Continuity of the shear strain implies:

$$\frac{P_1}{\eta E_i t_i \beta_n} = A_{n-1}\sinh\left(\beta_{n-1} l\right) + B_{n-1}\cosh\left(\beta_{n-1} l\right). \tag{47}$$

The total load transferred from the inner adherend to each of the outer adherends is:

$$\sum_{j=1}^{n-1} F_j + \frac{P_1}{E_i t_i \beta_n^2} \,. \tag{48}$$

Therefore, all that remains is to find $\mathbf{B_i}$ and then all other coefficients can be found from equations **41** and **45** and $\mathbf{P_1}$ can be found from equation **47**. A computerised iterative scheme was again implemented in which repeated estimates were made of $\mathbf{B_1}$ and the load transferred to the outer adherends calculated (from equation **48**) until that value was to equal to $P\,\frac{E_o t_o}{2E_o n t_o + E_i t_i}$.

3.1.2. Comparison of the Elastic Model with an FE Analysis

An FE analysis of a stepped double-lap joint was set up in PAFEC. The model was similar, in terms of element type and spacing, to the end-tapered double-lap joint model. Once again, only one quarter of the joint needed to be modelled due to the symmetry of the joint.

The adhesive shear strain was again calculated by subtracting displacements across the adhesive layer and dividing by the adhesive thickness. Three joints were modelled and the table of their joint parameters and figure numbers are shown below. The figures show excellent agreement between the mathematical model and the FE results.

	Figure 11	Figure 12	Figure 13
E_o (MPa)	208,000	208,000	138,000
t_o (mm)	0.13	0.13	0.15
E_1 (MPa)	71,000	71,000	71,000
t_1 (mm)	6.36	6.36	6.36
n (no. steps)	10	10	10
l (mm)	3	5	5
P (N/mm)	2,000	2,000	2,667
G (MPa)	590	590	590
η (mm)	0.1	0.2	0.2

Table 4.

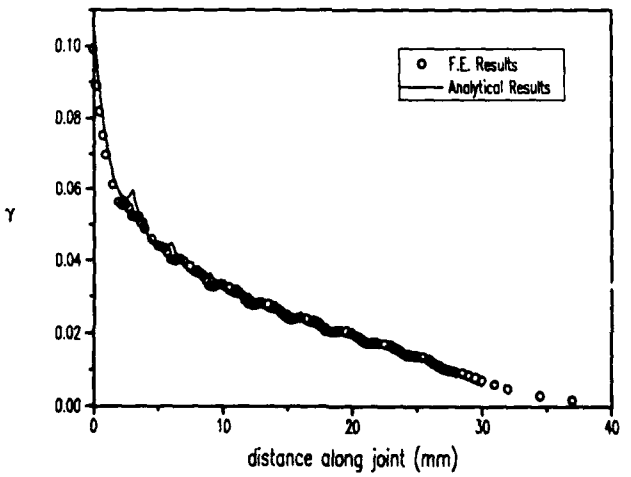

Figure 11.

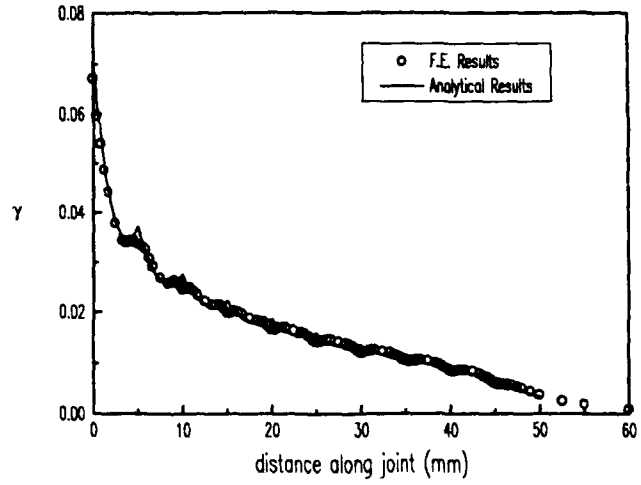

Figure 12.

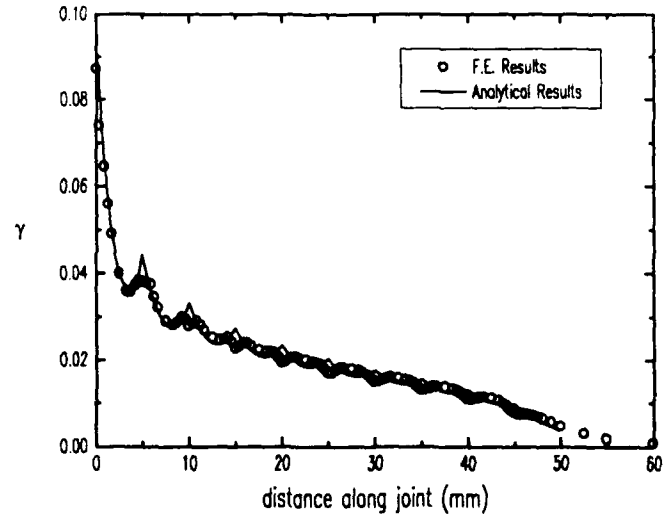

Figure 13.

3.1.3. An Upper and a Lower Bound for the Peak Shear Strain

Bounds for the peak shear strain in the adhesive assuming elastic deformation can be developed in much the same way as for the end-tapered double-lap joint. The lower bound is taken to be the adhesive shear strain when only one outer-adherend ply is present. The upper bound is taken to be the adhesive shear strain when all plies are present in a non-stepped geometry. Table five below has the parameters for this joint. The results are shown in figure 14.

P (N/mm)	Ei (MPa)	ti (mm)	Eo (MPa)	to (mm)	n	G (MPa)	η (mm)
1,500	71,000	6.36	205,000	0.13	5	750	0.13

Table 5.

The lower bound is quite sound for this joint configuration. The peak shear strain for this joint with a step length greater than 6 mm can be readily approximated by a joint having a single outer-adherend ply. This step length is equivalent to a taper angle of about 1.2°. A typical step length is about 3 mm (2.6°) in which case the lower bound underestimates the peak shear strain by about 20%.

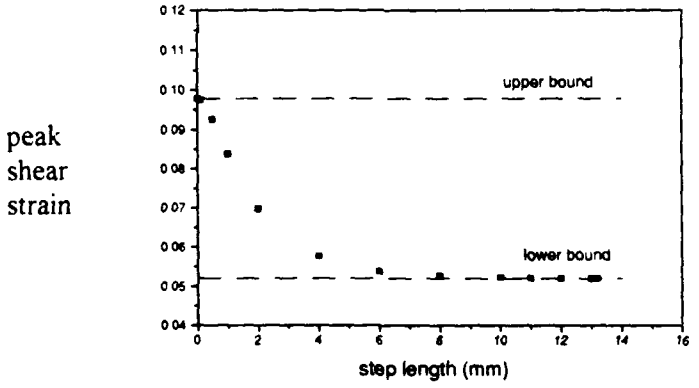

Figure 14.

3.2. Elastic/Perfectly-Plastic Analysis

3.2.1. Analytical Development

Solving for the elastic perfectly-plastic adhesive shear strain distribution in a stepped double-lap joint is similar to solving that for the elastic case except that the adhesive under each step can now also deform fully plastically or partly plastically and partly elastically.

The solution assuming perfectly-plastic adhesive deformation on the kth step is as given by equation 35:

$$\gamma_k\left(\xi\right) = \frac{\tau_p \beta_k^2 \xi^2}{2G} + C\xi + D, \tag{49}$$

where ξ is a local coordinate for each step. The boundary condition given by equations **11** still applies. Hence, on the first step the constant C in the above equation is:

$$C = -\frac{P}{\eta E_i t_i} \tag{50}$$

If on any step there is a transition from plastic-to-elastic adhesive deformation then the shear strain and its derivative given by equation **50** is matched with the elastic solution (equation **37**). At the end of each step continuity of the shear strain is enforced.

The derivative of the shear strain at the start of the **k**th step is given by equation **41**:

$$\frac{d\gamma_k}{d\xi}(0) = \frac{1}{\eta}\left(\frac{T_o}{k E_o t_o} - \frac{T_i}{E_i t_i}\right). \tag{51}$$

The traction $\mathbf{T_o}$ at the start of **k**th step is found by integrating equation **1** for the previous **k-1** steps. The traction $\mathbf{T_i}$ is simply equal to $\mathbf{P-2T_o}$. Thus once the shear strain at the start of the first step is known the full solution can be found.

Once again a computerised iterative scheme was implemented whereby repeated guesses were made at the starting shear strain until the load transferred was equal to $P\frac{E_o t_o}{2E_o n t_o + E_i t_i}$.

4. COMPARISON OF THE END-TAPERED AND THE STEPPED DOUBLE-LAP JOINT MODELS

4.1. Assuming Elastic Adhesive Deformation.

Table 6 contains the joint parameters used in the model of an end-tapered double-lap joint and in the model of an equivalent stepped double-lap joint assuming elastic adhesive deformation. The adhesive shear strains and outer adherend strains for these two joints appear in the figures that follow.

		Figures 15 and 16
End-tapered Double-Lap Joint	θ (degrees)	2.7
	l (mm)	27
	t_o° (mm)	0.13
Stepped Double-Lap Joint	t_o (mm)	0.13
	n (no. steps)	10
	step length (mm)	3

Table 6.

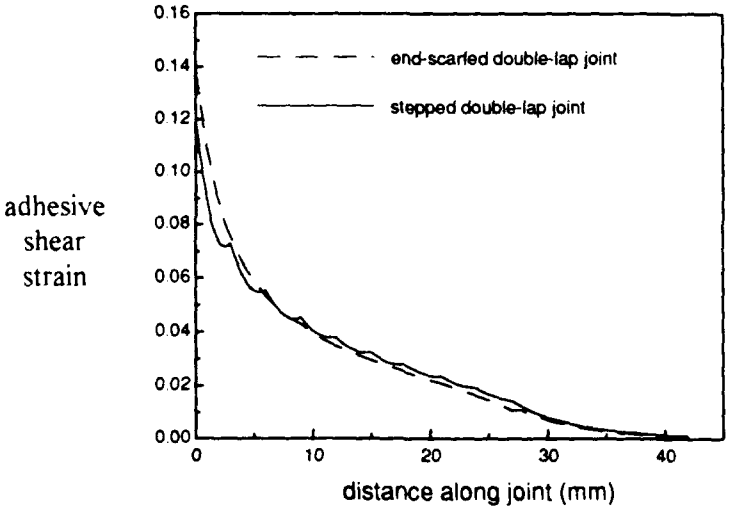

Figure 15.

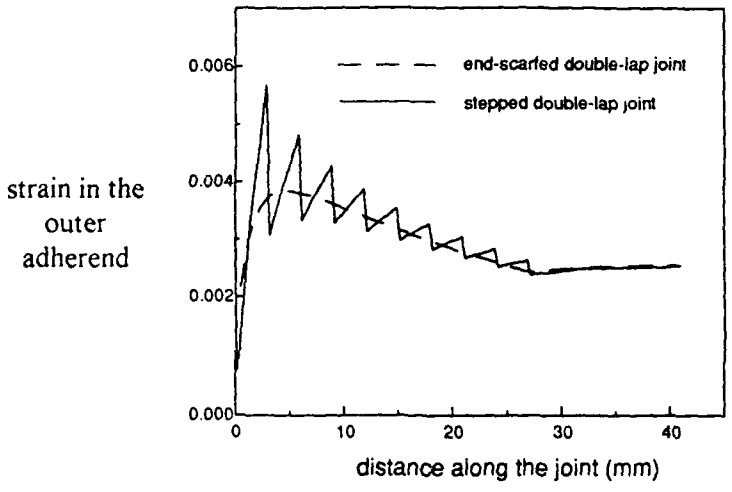

Figure 16.

Significantly, however, the stepped double-lap joint does predict a lower peak shear strain. The outer adherend strains are close in an average sense.

4.2. Assuming Elastic/Perfectly-Plastic Adhesive Deformation.

Table 7 contains the joint parameters used in the model of an end-tapered double-lap joint and in the model of an equivalent stepped double-lap joint assuming elastic/perfectly-plastic adhesive deformation. The adhesive shear strains and outer adherend strains for these two joints appear in the figures that follow.

		Figures 17 and 18
End-tapered Double-Lap Joint	θ (degrees)	2.9
	l (mm)	27
	t_o° (mm)	0.15
Stepped Double-Lap Joint	to (mm)	0.15
	n (no. steps)	10
	step length (mm)	3

Table 7.

Allowing the adhesive to deform in an elastic/perfectly-plastic manner leads to a slight divergence but still similar prediction of the adhesive shear strains by the two models. The predicted outer adherend strains for the two joints remain close in an average sense.

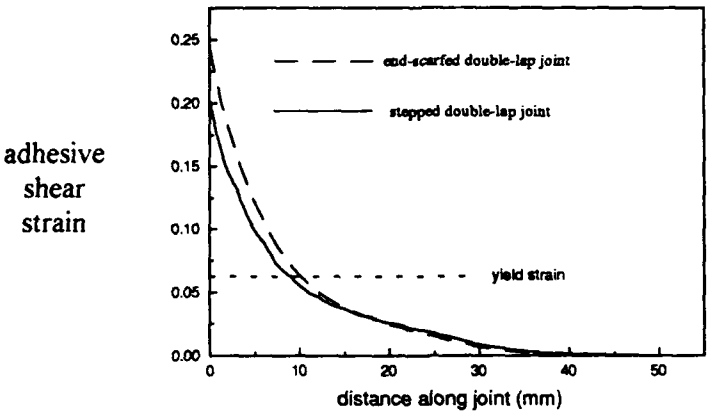

Figure 17.

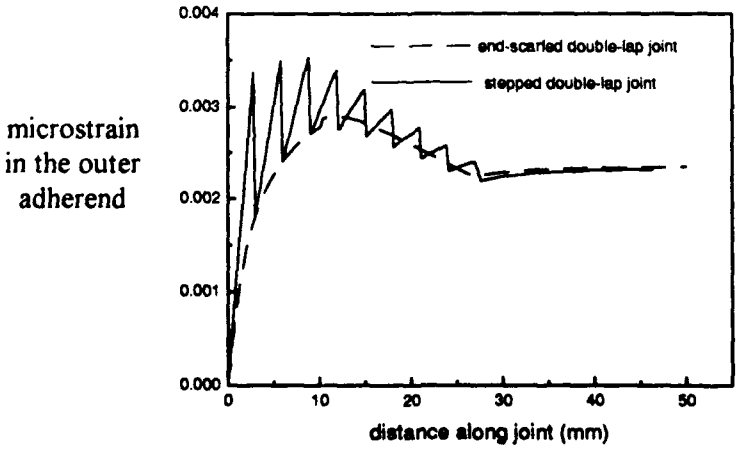

Figure 16.

4.3. Comparison of the Two Models with Measured Outer-Adherend Strains

The ability of the two models to predict strain in the outer adherend of an actual joint (Figure 1c) was investigated. A strip of strain gauges was bonded to the outer adherend of a boron/epoxy doubler near the end of the taper. The joint was loaded and the strain measured. The results and the predicted strains (calculated using the elastic models) are shown in Figure 19.

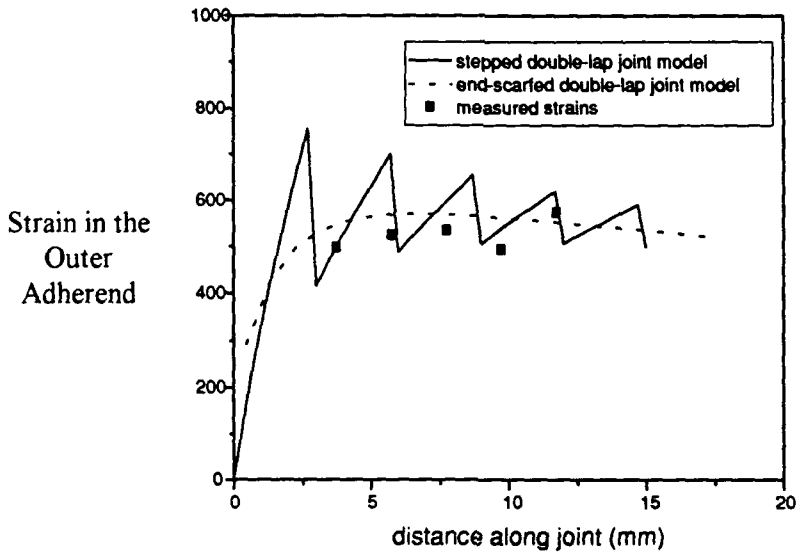

Figure 19.

Clearly, the stepped structure of the doubler is reflected in the strain measured on the outer ply. The stepped double-lap joint model is better suited to describing the lack of smoothness in the strain/distance curve though the end-tapered model is accurate in an average sense. The boron/epoxy doubler consisted of 10 plies and a step length of 3mm. The resultant taper angle was about 2.5°. Five strain gauges were bonded to the doubler: the strain gauges were spaced 2mm apart starting at 3mm from the end of the doubler.

5. CONCLUSION

Two alternative mathematical models have been successfully developed to predict adhesive shear strains in fibre-composite reinforcements. The validity of both the end-tapered double-lap joint model and the stepped double-lap joint model has been verified by an elastic finite-element analysis. For a typical repair or doubler geometry the two models yield approximately the same adhesive shear strains for both elastic and elastic/perfectly plastic analyses. The end-tapered double-lap joint model is numerically more stable than the stepped double-lap joint model and is perhaps therefore more useful in predicting adhesive shear strains. The stepped double-lap joint model, however, gives a better prediction of the strains in the outer adherend. Estimation of the peak shear strain in the stepped double-lap joint may be simplified by using a single ply model for certain joint

configurations. The stepped double-lap joint geometry appears to be more effective for repair than the end-tapered double-lap joint geometry as the predicted peak shear stress is lower. The two models could be useful design tools when used in conjunction with adhesive design allowables such as the fatigue threshold, the yield strain, and the strain to failure.

6. ACKNOWLEDGMENTS

The author wishes to acknowledge useful discussions with Dr. A. A. Baker on aspects of modelling the end-tapered double-lap joint.

7. REFERENCES

1. A.A. Baker, "Repair of Cracked or Defective Metallic Aircraft Components with Advanced Fibre Composites - an Overview of Australian Work", Composite Structures 2, pp. 153-181, 1984.

2. A.A. Baker, R.J. Chester, M.J. Davis, J.A. Retchford, and J.D. Roberts, "The Development of a Boron/Epoxy Doubler System for the F111 Wing Pivot Fitting - Materials Engineering Aspects", International Conference on Aircraft Damage Assessment and Repair, The Institute of Engineers, Australia, National Conference Publication no. 91/17, August 1991.

3. S.W. Tsai, "Composite Design-4th Edition", Think Composites, Dayton, Ohio, 1988.

4. L.J. Hart-Smith, "Adhesive-Bonded Double-Lap Joints", Douglas Aircraft Co., NASA Langley Report CR-11234, January 1973.

DISTRIBUTION

AUSTRALIA

Department of Defence

Defence Central

Chief Defence Scientist
AS, Science Corporate Management } shared copy
FAS Science Policy
Counsellor, Defence Science, London (Doc Data sheet only)
Counsellor, Defence Science, Washington (Doc Data sheet only)
S.A. to Thailand MRD (Doc Data sheet only)
S.A. to the DRC (Kuala Lumpur) (Doc Data sheet only)
Scientific Adviser, Defence Central
OIC TRS, Defence Central Library
Document Exchange Centre, DSTIC (8 copies)
Defence Intelligence Organisation
Librarian, Defence Signals Directorate, (Doc Data sheet only)

Aeronautical Research Laboratory

Director
Library
Chief Airframes and Engines Division
Author: Peter Chalkley
Dr Alan Baker
Dr Richard Chester

Materials Research Laboratory

Director/Library

Defence Science & Technology Organisation - Salisbury

Library

Navy Office

Navy Scientific Adviser (3 copies Doc Data sheet only)
Aircraft Maintenance and Flight Trials Unit
Director Aircraft Engineering - Navy
Naval Support Command
Superintendent, Naval Aircraft Logistics

Army Office

Scientific Adviser - Army (Doc Data sheet only)
Engineering Development Establishment Library
US Army Research, Development and Standardisation Group (3 copies)

Air Force Office
Air Force Scientific Adviser
Aircraft Research and Development Unit
Library
DGLP-AF
AHQ (SMAINTSO)
DGELS AIRREG4 HQLC
DGELS (OIC AME)
OIC ATF, ATS, RAAFSTT, WAGGA (2 copies)

HQ ADF
Director General Force Development (Air)

Other Organisations
NASA (Canberra)
AGPS

Department of Transport & Communication
Library

Statutory and State Authorities and Industry
ASTA Engineering, Document Control Office
Ansett Airlines of Australia, Library
Australian Airlines, Library
Qantas Airways Limited
Civil Aviation Authority
Hawker de Havilland Aust Pty Ltd, Victoria, Library
Hawker de Havilland Aust Pty Ltd, Bankstown, Library
BHP, Melbourne Research Laboratories

Universities and Colleges
Adelaide
Professor Mechanical Engineering

Flinders
Library

LaTrobe
Library

Melbourne
Engineering Library

Monash
Hargrave Library
Head, Materials Engineering

Newcastle
Library
Professor R. Telfer, Institute of Aviation

New England
Library

Sydney
Engineering Library
Head, School of Civil Engineering

NSW
Head, Mechanical Engineering
Library, Australian Defence Force Academy

Queensland
Library

Tasmania
Engineering Library

Western Australia
Library
Head, Mechanical Engineering

RMIT
Library
Mr M.L. Scott, Aerospace Engineering

University College of the Northern Territory
Library

UNITED KINGDOM
Defence Research Agency (Aerospace)
Materials and Structures Department
Mr Richard Potter

UNITED STATES OF AMERICA
Naval Air Warfare Center - Aircraft Division
R.L. Trabocco
Douglas Aircraft Company
L.J. Hart Smith MDC Fellow

SPARES (4 COPIES)

TOTAL (74 COPIES)

AL 149 DEPARTMENT OF DEFENCE

DOCUMENT CONTROL DATA

PAGE CLASSIFICATION
UNCLASSIFIED

PRIVACY MARKING

1a. AR NUMBER	1b. ESTABLISHMENT NUMBER	2. DOCUMENT DATE	3. TASK NUMBER
AR-008-365	ARL-RR-7	MAY 1993	AIR 92/089

4. TITLE

MATHEMATICAL MODELLING OF BONDED FIBRE-COMPOSITE REPAIRS TO AIRCRAFT

5. SECURITY CLASSIFICATION (PLACE APPROPRIATE CLASSIFICATION IN BOX(S) IE. SECRET (S), CONF. (C) RESTRICTED (R), LIMITED (L), UNCLASSIFIED (U)).

DOCUMENT	TITLE	ABSTRACT
U	U	U

6. NO. PAGES: 28

7. NO. REFS.: 4

8. AUTHOR(S)

P.D. CHALKLEY

9. DOWNGRADING/DELIMITING INSTRUCTIONS

Not applicable.

10. CORPORATE AUTHOR AND ADDRESS

AERONAUTICAL RESEARCH LABORATORY

AIRFRAMES AND ENGINES DIVISION

506 LORIMER STREET

FISHERMENS BEND VIC 3207

11. OFFICE/POSITION RESPONSIBLE FOR:

SPONSOR RAAF DTECHSPT-LC

SECURITY -

DOWNGRADING -

APPROVAL CAED

12. SECONDARY DISTRIBUTION (OF THIS DOCUMENT)

Approved for public release.

OVERSEAS ENQUIRIES OUTSIDE STATED LIMITATIONS SHOULD BE REFERRED THROUGH DSTIC, ADMINISTRATIVE SERVICES BRANCH, DEPARTMENT OF DEFENCE, ANZAC PARK WEST OFFICES, ACT 2601

13a. THIS DOCUMENT MAY BE ANNOUNCED IN CATALOGUES AND AWARENESS SERVICES AVAILABLE TO ....

No limitations.

13b. CITATION FOR OTHER PURPOSES (IE. CASUAL ANNOUNCEMENT) MAY BE [X] UNRESTRICTED OR [ ] AS FOR 13a.

14. DESCRIPTORS

Aircraft repair
Fatigue damage repair
Bonded composite repairs
Doublers (repair)

15. DISCAT SUBJECT CATEGORIES

0103

16 ABSTRACT

Bonded fibre-composite doublers are increasingly being used to reinforce and/or repair damaged or underdesigned metallic aircraft structure. This trend will continue as the average age of Australian civilian and military aircraft increases. Two mathematical models of the stress state in bonded doublers are presented in this report: the end-tapered double-lap joint and the stepped double-lap joint. The mathematical development of the two models is detailed and the fidelity of the predicted stress states compared with that obtained from finite element analyses and experiment.

PAGE CLASSIFICATION
UNCLASSIFIED
PRIVACY MARKING

THIS PAGE IS TO BE USED TO RECORD INFORMATION WHICH IS REQUIRED BY THE ESTABLISHMENT FOR ITS OWN USE BUT WHICH WILL NOT BE ADDED TO THE DISTIS DATA UNLESS SPECIFICALLY REQUESTED.

16. ABSTRACT (CONT).

17 IMPRINT

AERONAUTICAL RESEARCH LABORATORY, MELBOURNE

18. DOCUMENT SERIES AND NUMBER	19. WA NUMBER	20. TYPE OF REPORT AND PERIOD COVERED
Research Report 7	36 341B	

21 COMPUTER PROGRAMS USED

22. ESTABLISHMENT FILE REF.(S)

23 ADDITIONAL INFORMATION (AS REQUIRED)